On the applicability limits of double-sided self-pierce riveting

Alves, Luis M.; Moghadam, Marcel; Afonso, Rafael M.; Nielsen, Chris; Martins, Paulo A. F.

Published in:
Proceedings of the Institution of Mechanical Engineers, Part L: Journal of Materials: Design and Applications

Link to article, DOI:
10.1177/14644207221093627

Publication date:
2022

Document Version
Peer reviewed version

On the Applicability Limits of Double-Sided Self-Pierce Riveting

Luis M. Alves[1], Marcel Moghadam[2], Rafael M. Afonso[1], Chris V. Nielsen[3], Paulo A.F. Martins[(1)]*

[1]IDMEC, Instituto Superior Técnico, Universidade de Lisboa,
Av. Rovisco Pais, 1049-001 Lisboa, Portugal

[2]Department of Mechanical Engineering, Technical University of Denmark,
2800 Kgs. Lyngby, Denmark (now with Convatec, 4320 Lejre, Denmark)

[3]Department of Mechanical Engineering, Technical University of Denmark,
2800 Kgs. Lyngby, Denmark

(*) Corresponding author. E-mail: pmartins@tecnico.ulisboa.pt
First author. E-mail: luisalves@tecnico.ulisboa.pt
Second author. E-mail: marcel.moghadam@convatec.com
Third author. E-mail: rafael.afonso@tecnico.ulisboa.pt
Fourth author: E-mail: cvni@mek.dtu.dk

ABSTRACT

This paper revisits double-sided self-pierce riveting to discuss the applicability limits related to the thickness of the sheets to be used in hidden lap joint connections. Special emphasis is given to thin sheets with thicknesses that are significantly smaller than those earlier reported in the literature. The overall methodology draws from experimental and numerical simulation to aspects related to the working principle of double-sided self-pierce riveting and geometric scalability of the chamfered tubular rivets. Results show that double-sided self-pierce riveting can be successfully applied in thin sheets and must be seen as an alternative to well-established joining processes such as conventional self-pierce riveting and resistance spot welding. In case of the latter, comparisons are made against double-sided self-pierce riveting regarding the force and energy requirements to assemble and destroy the resulting lap joints. Destruction of the joints is performed by means of shear tests and provides the maximum force and energy that both types of lap joints are capable to withstand without failure.

Keywords: Joining by forming, Thin-metal sheets, Double-sided self-pierce riveting, Resistance spot welding, Experimentation, Finite element method.

1. INTRODUCTION

In recent years, double-sided self-pierce riveting (DSSPR) has been developed with the aim of becoming an alternative to self-pierce riveting (SPR) for applications that require lap joint connections between sheets to be invisible from both surface sides. The process was proposed by Kato et al. [1], who replaced the semi-tubular rivets of SPR (Fig. 1a) [2], by tubular rivets with chamfered ends placed in-between the sheets to be joined and subsequently pierced through by compression with flat dies (Fig. 1b).

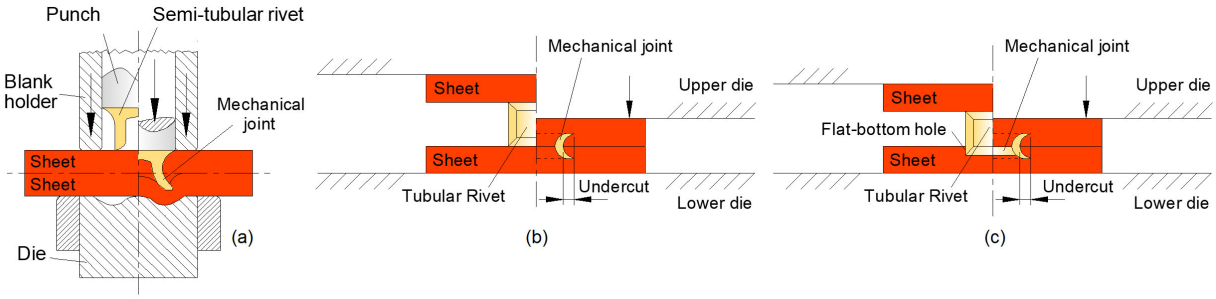

Fig. 1 Schematic representation of the working principle of (a) self-pierce riveting (SPR), (b) double-sided self-pierce riveting (DSSPR) and (c) double-sided self-pierce riveting (DSSPR) with flat-bottom holes.

SPR and DSSPR belong to the category of joining by forming processes with auxiliary elements (rivets) [3]. Their working principle is based on the creation of form-closed joints built upon mechanical interlocks that hold the overlapped sheets tightly together. The original developments of DSSPR by Kato et al. [1] in the early 2000's made use of aluminium sheets with 3 mm thickness and stainless-steel tubular rivets with chamfered ends. The chamfered rivet ends flare during piercing through the sheets to create the essential undercuts that are necessary to produce form-closed joints (Fig. 1b). The work showed that stainless-steel tubular rivets of 0.5 mm and 0.75 mm wall thickness with chamfered ends of 45° to 60° could be successfully applied to produce hidden lap joint connections (hereafter referred to as 'lap joints', or simply 'joints') and to avoid the

formation of material protrusions above and below the upper and lower sheet surfaces. These last two features, which are not available in SPR, stimulated other researchers to further develop DSSPR and foster its potential use in joining by forming applications.

Huang et al. [4], for example, showed that DSSPR can give rise to asymmetric lap joints whenever the rivets are incorrectly positioned and aligned with the sheets or have obliquities resulting from their fabrication process. The work made use of aluminium AA6063 sheets with 2.4 mm thickness and AISI 304 stainless-steel tubular rivets with 0.8 mm thickness and suggests the inclusion of outer [4] or inner flanges [5] at the mid tubular rivet height to reduce the risk of obtaining asymmetric joints. However, the new geometry of the rivets comes with the price of increasing the complexity and production costs of the rivets.

In view of the above, Alves et al. [6] proposed the preliminary machining of flat bottom holes in the strongest sheet to correctly position the tubular rivets (without flanges) before piercing (Fig. 1c). The validation work was performed in aluminium AA5754 and polyvinylchloride (PVC) sheets with 5 mm thickness using AISI 304 stainless steel tubular rivets having 1.5 mm wall thickness and allowed the following two conclusions to be reached. Firstly, the new proposed variant of DSSPR with flat bottom holes is effective to diminish the risk of producing asymmetric joints. Secondly, the need of using tubular rivets with different chamfered angles of 30° and 60° to compensate the greater or lesser difficulty to pierce through sheets of dissimilar materials with different mechanical strengths.

The above-mentioned conclusion regarding the capability of DSSPR to produce lap joints in sheets made from dissimilar materials adds to several other features and advantages that make DSSPR a valuable alternative to SPR, such as:

(i) the capability of producing hidden lap joint connections,

(ii) the avoidance of material protrusions above and below the upper and lower sheet surfaces,

(iii) the capability of being used in thick sheets because the joining mechanism avoids tearing up the sheets placed on the punch side,

(iv) the avoidance of the need to position the thinner and/or softer sheets on the punch side, as a corollary of (iii).

As the overall applicability of SPR is generally limited to lap joints with a total thickness from about 1.5 mm to 6 mm in steel and up to 10 mm in lightweight alloys [7], and because there is no upper thickness limit in DSSPR, the question that still needs to be answered has to do with its applicability to produce lap joints in thin sheets. In fact, as far as the authors are aware, the minimum sheet thickness that has so far been reported in literature is 2.4 mm [4].

Under these circumstances, the first objective of this paper is to evaluate the possibility of using DSSPR to produce lap joints in thin sheets. This objective is directly related to the working principle and geometric scalability of the chamfered tubular rivets and is accomplished by means of a combined experimental and numerical simulation work.

The second objective is to compare the force and energy requirements to assemble and destroy the lap joints produced by DSSPR against alternative lap joints produced by resistance spot welding (RSW). The choice of RSW is justified by its wide industrial use in thin sheets [8]. The destruction of the joints is investigated by means of shear destructive tests.

2. METHODS AND PROCEDURES

2.1 Materials and flow curves

The work on DSSPR was carried out in commercial AA5754-H111 aluminium sheets with 1.5 mm thickness and the tubular rivets were machined from AISI 304 stainless-steel rods with a diameter of 10 mm.

The flow curve of the aluminium sheets is shown in Fig. 2 and was obtained from tensile and stack compression tests performed at ambient temperature in a hydraulic testing machine (Instron SATEC 1200 kN). The tensile tests specimens were extracted from the sheets in accordance with the ASTM standards E8/E8M [9]. The stack compression test specimens were obtained by pilling up cylindrical disks extracted from the sheets in accordance with a procedure that was previously utilized by the authors [10].

The flow curve of the stainless-steel rods is also shown in Fig. 2 and was obtained from compression tests performed in cylindrical specimens machined out from the rods. Both stack and conventional compression tests were carried out with a cross head speed of the hydraulic testing machine equal to 5 mm/min.

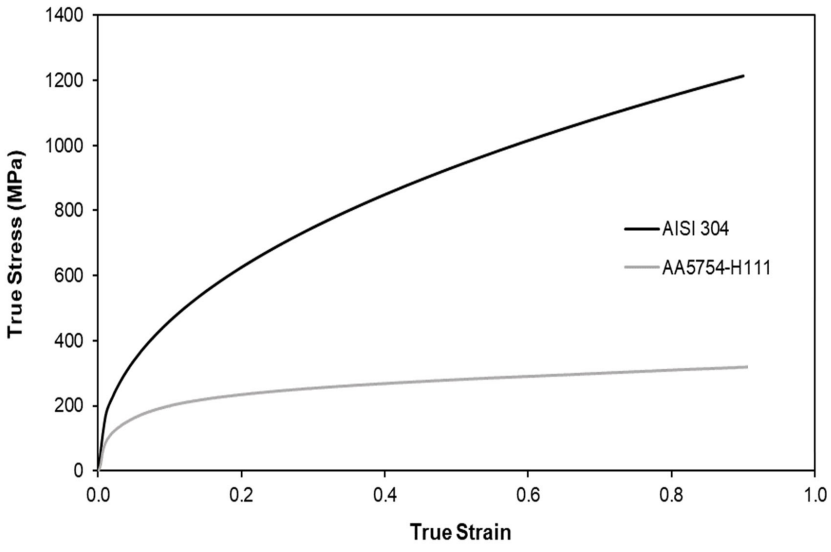

Fig. 2 Flow curves of the aluminium AA5754-H111 sheets and of the AISI 304 stainless-steel rivets.

2.2 Experimental work plan

The DSSPR experiments were carried out at ambient temperature in a servo mechanical press and gave rise to a permanent form-closed mechanical joint between the overlapped sheets. Even though DSSPR is a process whose development and application are still in its early stages when compared to other joining by forming processes such as SPR, it is important to point out that the joining process most widely used to produce lap joints in thin metal sheets is resistance spot welding [11].

Resistance spot welding (RSW) is classified as a joining by welding process [12] and uses electric power to locally heat and melt the material of the sheets into a nugget while they are pressed together by a pair of electrodes. Because RSW is utilized as a reference to compare the morphology of the connections and the required forces and energies to assemble and destroy the joints against those produced by DSSPR, it was decided to use a tubular rivet geometry (Fig. 3a) compatible with that of the welding nuggets (Fig. 3b). The main notation and process parameters of DSSPR and RSW are also included in Fig. 3.

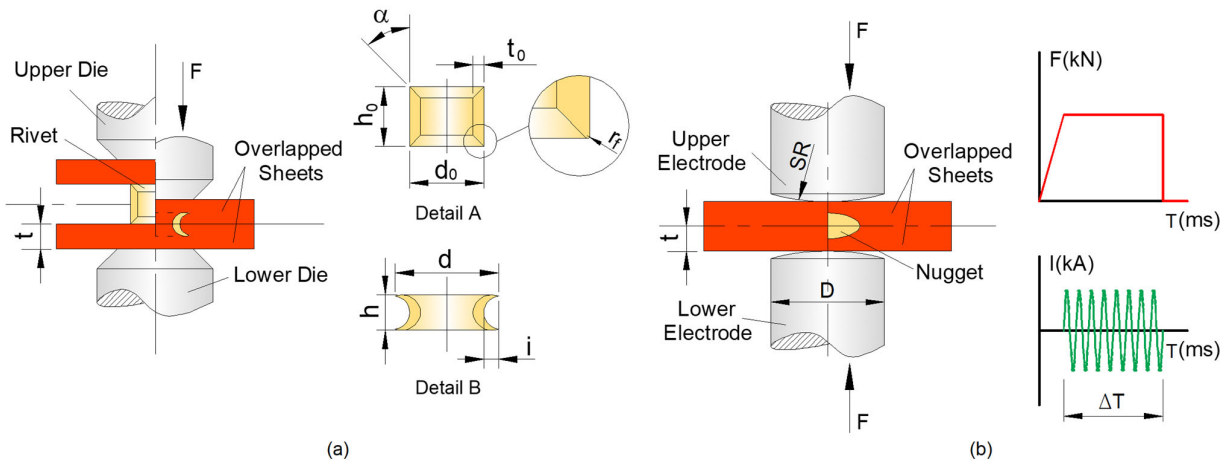

Fig. 3 Schematic representation of the two joining processes utilized in the experimental work plan:

(a) DSSPR with a detail of the tubular rivets before and after joining,
(b) RSW before and after joining with a detail of the evolution of the electrode force F and of the welding current I with process time T.

The RSW experiments were carried out in an 8105 Tecna 250kVA resistance welding machine with TE 180 control unit. The spot welding took place under an electrode force of 3.3 kN. The 50 Hz alternating current was delivered in a single pulse of 8 cycles. The RMS current was varied in the interval 25-35 kA to cover the best suitable welding current. The type A0 electrodes of ISO 5182 [13] class A2-2 material utilized in the tests had an outer diameter $D = 16$ mm and a rounded tip with sphere radius SR=40 mm (Fig. 3b), in accordance with the ISO 5821 standard [14].

Spot welding of 1.5 mm thick aluminium alloys is expected to result in weld nuggets with a diameter of approximately 6 mm [8]. Thus, to compare the connections produced by the two different types of joining processes, it was decided to perform the DSSPR experiments with tubular rivets having initial outer diameters d_0 equal to 4, 6 and 8 mm. Thereby, riveted connections with diameters smaller, similar, and larger than the spot welds will be tested.

The remaining process parameters of DSSPR that are shown in Fig. 3a such as: (i) the sheet thicknesses t, (ii) the height h_0, (iii) the wall thickness t_0, and (iv) the chamfered angle α of the rivet ends were kept constant because their influence was already investigated by the authors [15, 16]. This allowed utilizing the above-mentioned variations of d_0 to analyze the geometric scalability of the tubular rivets and its influence in the process working principle.

Table 1 summarizes the experimental work plan utilized in the DSSPR and in the reference RSW experiments. The symbols F, f, I_{RMS} and ΔT included in the table denote the electrode force, the frequency of the alternating current, the root mean square of the electric current and the welding time during which the electric current flowed between the two RSW electrodes, respectively (Fig. 3b). At least four specimens were produced for each combination of parameters included in Table 1.

Table 1 Summary of the main operating parameters utilized in the DSSPR and RSW experiments (notation in accordance with Fig. 3).

Sheet	t (mm)	width (mm)		length (mm)		
AA5754-H111	1.5	30		105		
DSSPR						
Rivet	d_0 (mm)	h_0 (mm)		t_0 (mm)	α (°)	
AISI 304	4, 6, 8	3		0.5	45	
RSW						
Electrode	D (mm),	SR (mm)	F (kN)	f (Hz)	I_{RMS} (kA)	ΔT (ms)
Type A0, class A2-2	16 mm	40mm	3.3	50	25-35	160 (8 cycles)

After completion of the DSSPR and RSW experiments, selected test specimens were halved lengthwise, to observe and compare the connections obtained by the two different types of joining processes. In case of the RSW test specimens, etching of the spot welds was performed in 2.5% concentration of hydrofluoric acid for 60 seconds.

The remaining test samples were subjected to destructive shear tests to determine the force and energy that both type of joints can withstand before failure. The tests were performed in the servo mechanical press, where the DSSPR joints were produced, in accordance with ISO 14273 [17], and the results are given in section 3.3.

2.3 Numerical modelling

Revisiting the working principle of DSSPR and analysing the geometric scalability of the chamfered tubular rivets required numerical simulation with finite elements. In the present work, the authors made use of the in-house finite element computer program i- form [18], which is built upon the flow formulation and based on the following modified weak form of the quasi-static force equilibrium equations to include contact and sliding with friction between deformable objects,

$$\int_V \sigma'_{ij}\delta D_{ij}dV + \int_V \sigma_m\,\delta D_v\,dV - \int_{S_t} t_i\,\delta u_i dS + \int_{S_f}\left(\int_0^{|u_r|}\tau_f \delta u_r\right)dS + K_1\sum_{c=1}^{N_c} g_n^c \delta g_n^c = 0 \quad (1)$$

The flow formulation makes use of a kind of 'updated Eulerian' approach [19] since the finite element equations resulting from (1) are written in the current (deformed) configuration and use a control volume with velocities u_i as the primary unknowns.

The deviatoric Cauchy stress σ'_{ij}, the hydrostatic stress σ_m, the rate of deformation D_{ij} and the volumetric rate of deformation D_v included in (1), make the computer implementation similar to that of a viscous fluid subjected to relaxation of the incompressibility condition $D_v = 0$ by means of a penalty function K, with $\sigma_m = (K/2)D_v$. The remaining symbols in (1) denote the tractions t_i applied on the boundary S_t of the control volume, and the friction shear stress τ_f and the relative sliding velocity u_r acting on the contact interfaces S_f between the deformable and rigid objects. Friction is included in the finite element model by means of the law of constant friction $\tau_f = mk$, where k is the shear flow stress and m is the friction factor. A friction factor equal to 0.1 was used after checking the predicted finite element riveting forces that best matched the experimental forces.

The last term of (1) accounts for the contact between deformable objects by means of a two-pass contact search algorithm. The symbols N_c and g_n^c denote the contact pairs and the corresponding normal gap velocities, which are penalized by a large number K_1 to avoid penetration, as it is comprehensively explained in [20].

Figure 4 shows a typical finite element model used in the numerical simulation of DSSPR at the beginning and end of the joining process. The model considered plastic deformation resulting from piercing and flaring of the rivets through the sheets to be axisymmetric and is built upon three deformable objects (the rivet and the upper and

lower sheets) and two rigid objects (the upper and lower flat tools). The cross-section of the deformable objects (rivet and sheets) was discretized by means of approximately 12000 quadrilateral elements whereas the cross-section of the rigid objects (tools) was discretized by means of linear contact-friction elements.

According to the finite element flow formulation equilibrium was checked by means of an iterative procedure meant to minimise the residual of (1) to within a specified tolerance. A convergence criterion of the residual equal to 10^{-3} was utilized, after which the geometry was updated based on the calculated velocities. Remeshing was performed several times to repair and refine the meshes of the rivets as they were pierced through the sheets.

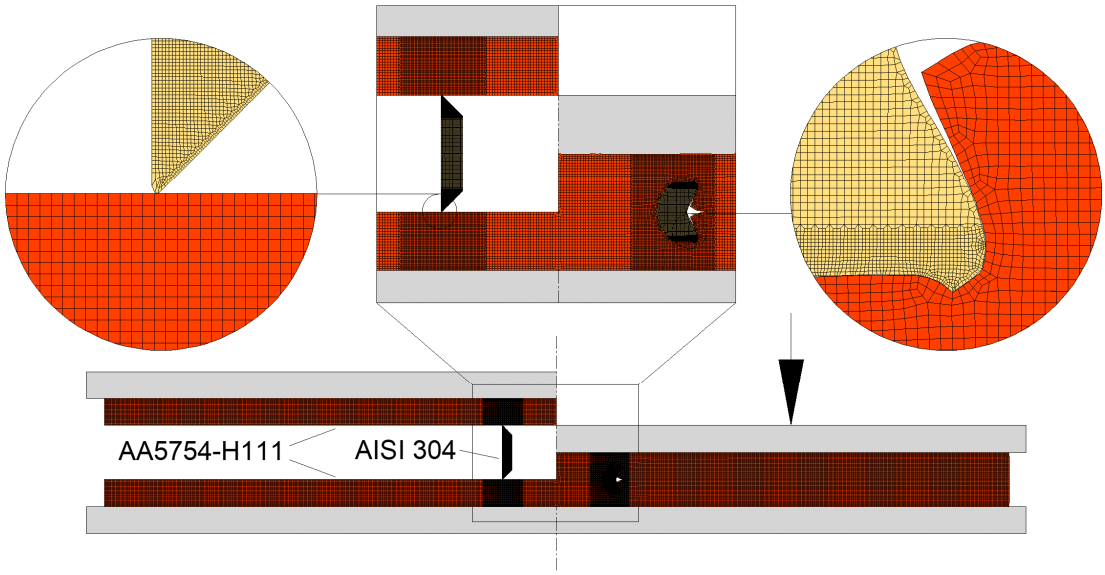

Fig. 4 Finite element model utilized in the numerical simulation of DSSPR at the beginning and end of joining ($d_0 = 6$ mm).

The computational time for a typical analysis on a computer equipped with an Intel i7-5930K CPU processor was approximately equal to 15 min.

3. RESULTS AND DISCUSSION

3.1 Working principle and scalability of double-sided self-pierce riveting

Figure 5 discloses the working principle of DSSPR by showing the finite element predicted cross-sections of the lap joints at the beginning, middle and end of the joining process. Three different plastic deformation stages are identified. An initial stage, during which the rivets are pressed through the sheets by the upper and lower dies (Fig. 5a). A second stage, where the rivets continue to be pressed through the sheets but in which piercing is accompanied by flaring of the rivet chamfered ends (Fig. 5b). A third final stage, where the two sheets get into contact and clamping by mechanical interlocking is obtained from the undercuts (refer to '*i*' in Fig. 3a) that were created by flaring of the chamfered tubular rivets.

The agreement between finite element predicted geometries (Fig. 5c) and photographs (Fig. 5d) of the final cross-sections is generally good, apart from a slight tendency of the numerical model to favour upsetting instead of flaring when the initial outer diameter d_0 increases from 4 to 8 mm. These differences are attributed to minor variations of the fillet radius r_f of the chamfered tube ends (refer to the detail in Fig. 3a) within the tolerances of fabrication because numerical models made use of the nominal dimensions of the tubular rivets instead of the actual dimensions for each specific test case.

Still, the results shown in Fig. 5 allow concluding on the overall suitability of the numerical model to replicate and help understanding the working principle of DSSPR.

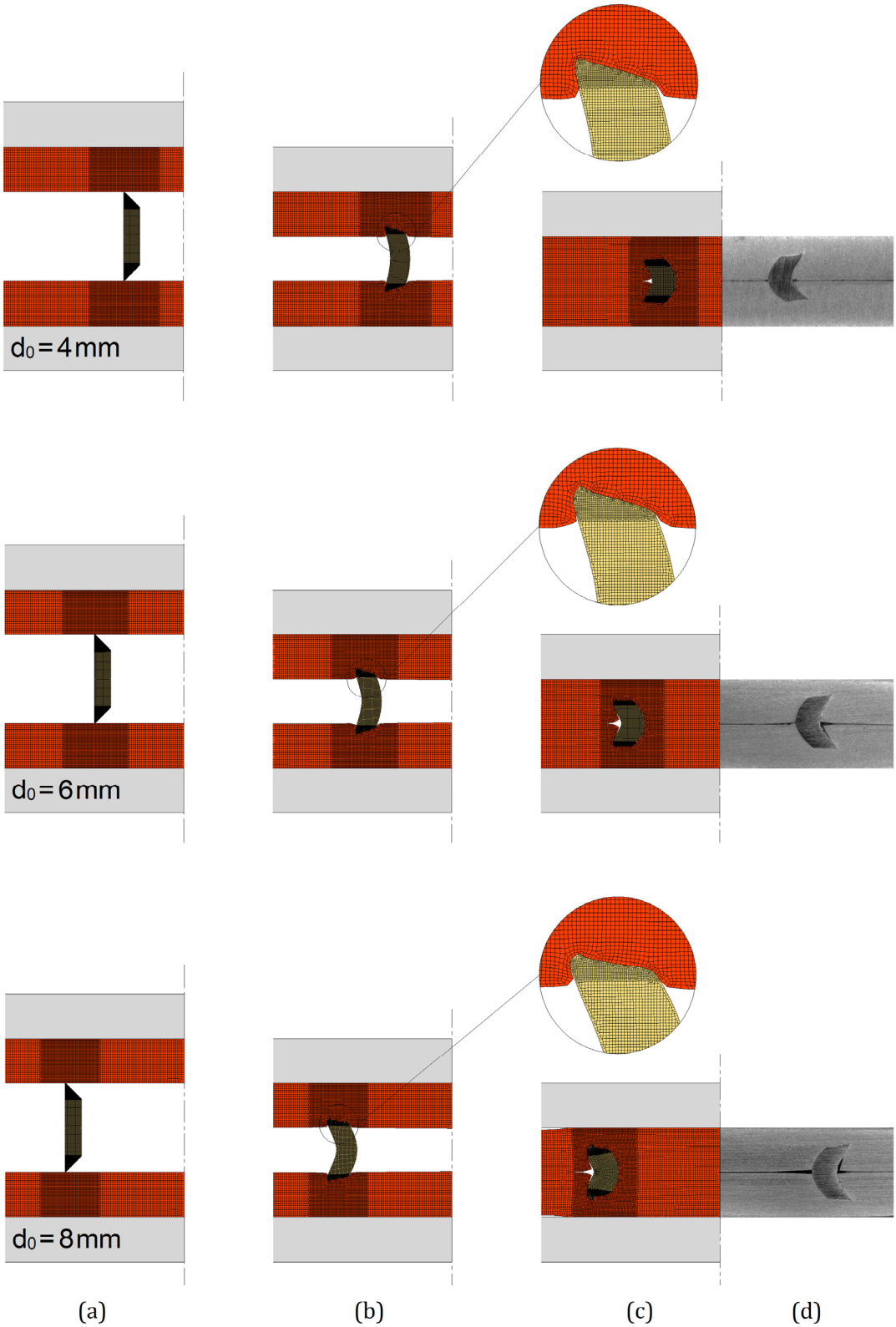

Fig. 5 Finite element predicted geometry of the cross-sections for tubular rivets with different initial outer diameters d_0 at the (a) beginning, (b) middle and (c) end of joining by DSSPR. Photographs of the cross-sections taken from the corresponding experimental test samples are given in (d).

Regarding geometric scalability of the tubular rivets due to an increase of their initial outer diameters d_0 from to 4 to 6 and 8 mm, both finite elements and photographs show that the differences in the amounts of piercing, flaring and undercut are negligible. This is compatible with keeping the same height, wall thickness and chamfer angle for all the specimens.

In fact, as will be shown in the following sections of the paper, major differences resulting from geometric scalability of the tubular rivets are found in the required forces and energies to assemble and destroy the resulting lap joints.

A comparison between the lap joints produced by DSSPR and RSW is provided in Fig. 6. As seen, the outer diameter of deformed rivet ($d_0 = 8$ mm) is close to that of the welding nugget, but while the RSW connection is ensured by the entire volume of the welding nugget, the DSSPR connection is solely ensured by the undercut resulting from piercing and flaring of the rivet tube wall, because joining by forming is carried out at ambient temperature without local heating and melting of the sheet material.

The absence of heating-cooling cycles caused by the passage of electric current also explains the reason why the surfaces of the lap joints produced by DSSPR are generally smooth (Fig. 6a) while those produced by RSW are not flat due to the local indentation marks of the electrodes used for pressing the sheets and applying the electric current (Fig. 6b).

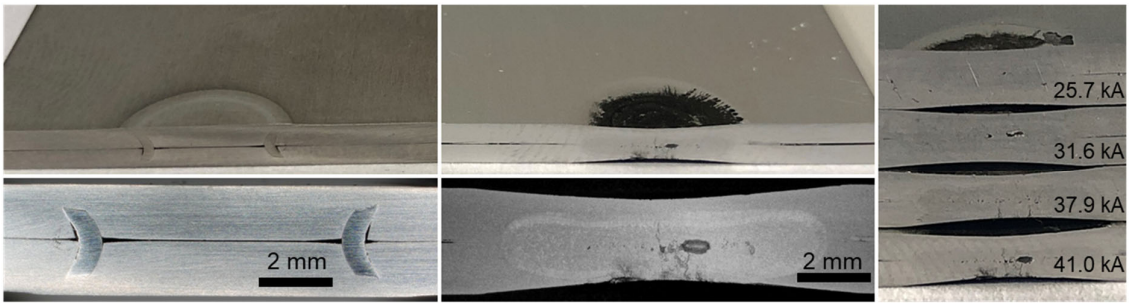

Fig. 6 Photographs with the top and cross-sectional views of the lap joints produced by (a) DSSPR ($d_0 = 8$ mm) and (b) RSW (41.0 kA). In (c) the evolution of electrode indentation is shown as function of welding current.

3.2 Riveting force and energy

Finite element predicted and experimental evolutions of the riveting force with the vertical displacement of the upper die are disclosed in Fig. 7. The results are provided for the three different outer diameters d_0 of the tubular rivets under analysis and allow identifying the three different plastic deformation stages of DSSPR that were described in the previous section.

The initial stage corresponds to indentation under growing wall thickness due to piercing of the chamfered rivet ends. This region is labelled as 'I' in the graphic. The second stage, labelled as 'II', is characterized by a slight reduction in the force growing rate due to combination of piercing and flaring under a constant wall thickness of the rivets. The third and final stage labelled as 'III' starts when the two overlapped sheets are brought into contact and is characterized by a steep increase in the force as a consequence of the sheets start being pressed against each other.

The schematic drawings included in Fig. 7 allow further understanding the relation between process mechanics and riveting force vs. displacement evolution.

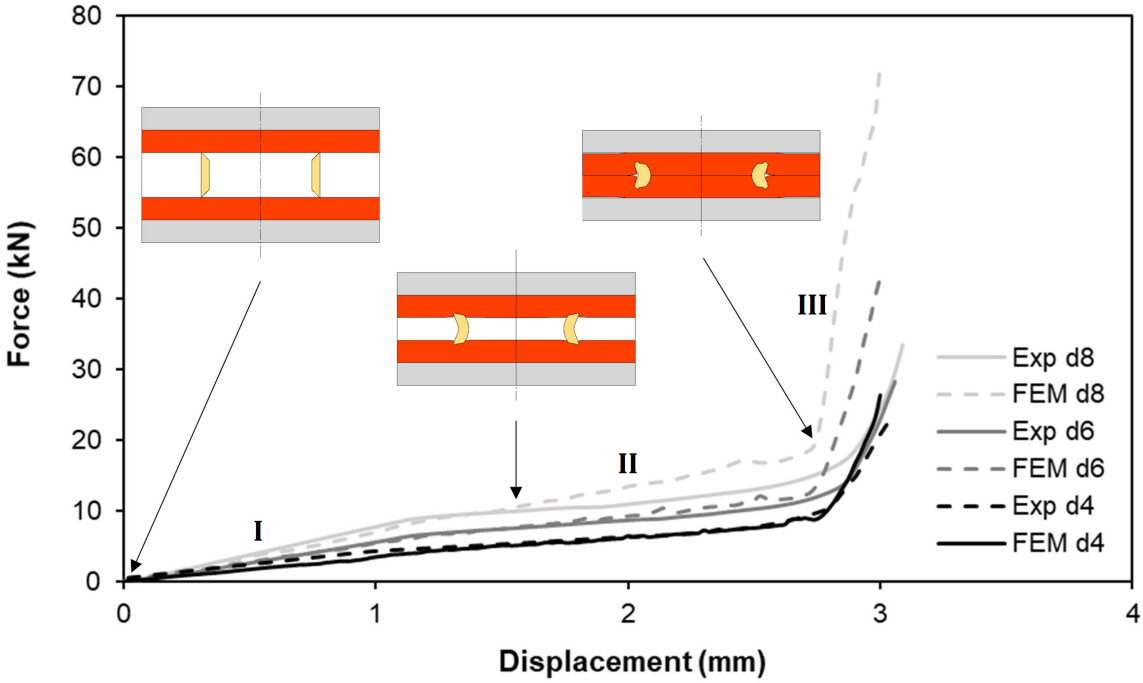

Fig. 7 Finite element predicted and experimental evolution of the riveting force with displacement for the three different outer diameters d_0 of the tubular rivets.

As seen in Fig. 7, the riveting forces, and the total required energy (area below the force vs. displacement curve) increase with the initial outer diameter d_0 of the tubular rivets. In fact, an increase of approximately 18% in the force and 64% in the total energy is obtained when the initial outer diameter d_0 of the rivets increases from 4 mm to 8 mm due to an increase of the cross-sectional area of the tubular rivet.

The comparison against the values obtained by RSW for different values of the RMS current I_{RMS} is provided in Fig. 8. As seen, while the riveting forces of DSSPR are about 6 to 7 times larger than those required by RSW, the total energies are 130 to 140 times smaller than those required by RSW.

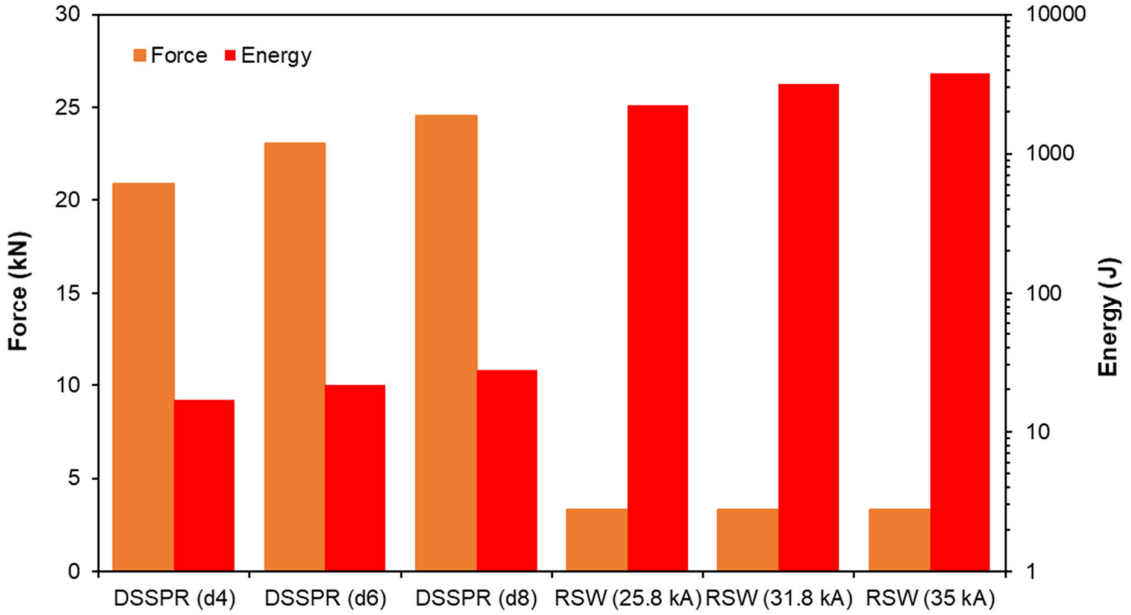

Fig. 8 Riveting forces and energies required by DSSPR and by RSW.

3.3 Destructive shear force and energy

The force and energy to destroy the lap joints fabricated by DSSPR and RSW were determined by means of destructive shear tests. The results are shown in Fig. 9 and allow concluding that lap joints produced by RSW required higher destructive shear forces and energies than those required by DSSPR joints.

The differences in force, which may reach values up to 3 times, are explained by the fact that the resistance to shear of the lap joints fabricated by RSW are ensured by a continuous nugget resulting from local heating and melting of the material of the two sheets, whereas the resistance of the lap joints fabricated by DSSPR is exclusively ensured by the undercuts of the tubular rivets.

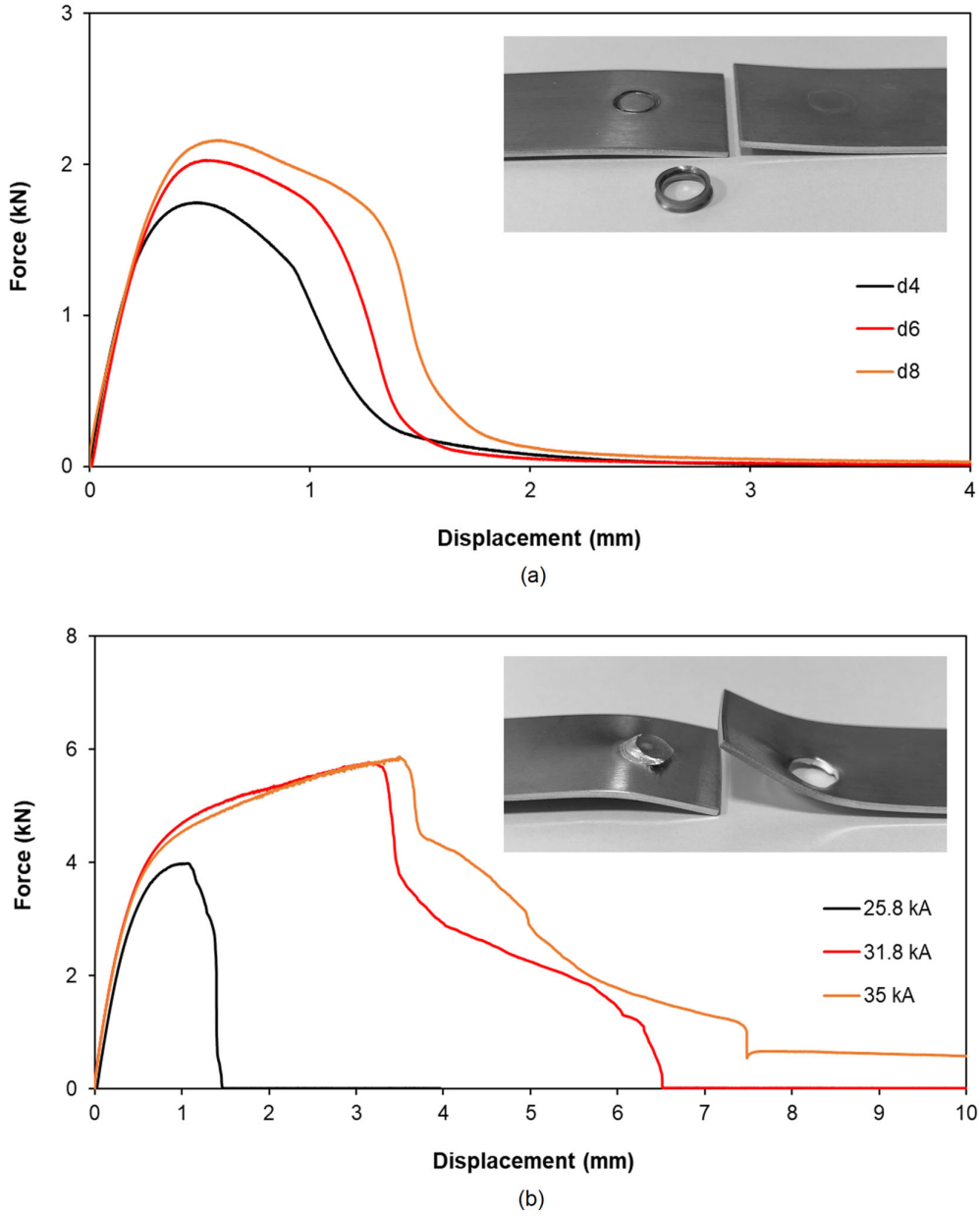

Fig. 9 Experimental evolution of the force with displacement for destructive shear tests performed on specimens produced by (a) DSSPR and (b) RSW. The enclosed photographs show details of the specimens after testing.

The highest energy absorption capacity of the lap joints fabricated by RSW with I_{RMS} values of 31.8 and 35 kA combined with the observed shift of the peak forces towards larger displacements are attributed to differences in the failure modes that are shown in the photographs included in Fig. 9. In fact, while the lap joints fabricated by RSW fail by

shearing along the length of the diameter of the nugget, the lap joints fabricated by DSSPR failed by bending and detachment of the tubular rivet from the overlapped sheets.

4. CONCLUSIONS

The main conclusions that can be drawn from the numerical and experimental work on the fabrication of lap joints by double-sided self-pierce riveting (DSSPR) are as follows:

- Chamfered tubular rivets can be scaled down in both height and outer diameter to allow fabricating lap joints in thin sheets with 1.5 mm thickness,
- The lap joints fabricated by DSSPR can ensure flat sheet surfaces with negligible material protrusions and no local indentation marks like, for example, in case of resistance spot welding (RSW), which is the most utilized joining process for thin sheets,
- Lap joining by DSSPR requires a significant less amount of energy than by RSW,
- The forces and energies required to destroy the lap joints fabricated by DSSPR are smaller than those of RSW because the failure mechanism prevailing in the destructive shear tests is based on bending and detachment of the rivets, instead of shearing,
- In contrast to RSW, DSSPR is carried out at ambient temperature and allows fabricating lap joints in thick sheets and in sheets made from dissimilar materials, as it was previously demonstrated by the authors [16].

ACKNOWLEDGMENTS

The authors would like to thank the support provided by Fundação para a Ciência e a Tecnologia of Portugal and IDMEC under LAETA-UIDB/50022/2020.

DECLARATION OF CONFLICTING INTERESTS

The authors declare that there is no conflict of interests.

REFERENCES

1. Kato, K., Okamoto, M., Yasuhara, T., 2001, Method of joining sheets by using new type of rivets. *Journal of Materials Processing Technology*, 111: 198-203.
2. Chrysanthou, A., Sun, X. (Ed.), 2014, *Self-piercing riveting: properties, processes, and applications*. Woodhead Publishing Limited, Cambridge, UK.
3. DIN 8593-5:2003-09, 2003, *Manufacturing processes joining - Part 5: Joining by forming processes; Classification, subdivision, terms and definitions*. DIN - German Institute for Standardization, Berlin
4. Huang, Z., Yao, Q., Lai, J., Zhao, J., Jiang, Z., 2017, Developing a self-piercing riveting with flange pipe rivet joining aluminum sheets. *International Journal of Advanced Manufacturing Technology*, 91: 2315-2328.
5. Huang, Z., Xue, S., Lai, J., Xia, L., Zhan, J., 2014, Self-piercing riveting with inner flange pipe rivet. *Procedia Engineering*, 81: 2042–2047.
6. Alves, L.M., Afonso, R.M., Pereira, P.T., Martins, P.A.F., 2021, Double-sided self-pierce riveting with flat-bottom holes: a feasibility study. *Production Engineering* https://doi.org/10.1007/s11740-021-01082-y
7. He, X., Pearson, I., Young, K., 2008, Self-pierce riveting for sheet materials: state-of-the-art. *Journal of Materials Processing Technology*, 199: 27–36.
8. Resistance Welding Manufacturers' Association, 2003, *Resistance welding manual*. RWMA, Philadelphia, USA.
9. ASTM E8/E8M, 2016, *Standard test methods for tension testing of metallic materials*. ASTM International, West Conshohocken, PA, USA..

10. Alves, L.M., Nielsen, C.V., Martins, P.A.F., 2011, Revisiting the fundamentals and capabilities of the stack compression test. *Experimental Mechanics*, 51: 1565–1572.
11. Bond, D., Suzuki, F.A., Scalice, R.K., 2020, Sheet metal joining selector. *Journal of the Brazilian Society of Mechanical Sciences and Engineering*, 42: 226
12. DIN 8593-6:2003-09, 2003, *Manufacturing processes joining - Part 6: Joining by welding; Classification, subdivision, terms and definitions*. DIN - German Institute for Standardization, Berlin
13. ISO 5182:2016, 2016, *Resistance welding - Materials for electrodes and ancillary equipment.* ISO - International Organization for Standardization, Geneva, Switzerland.
14. ISO 5821:2009(E), 2009, *Resistance welding – Spot welding electrode caps.* ISO - International Organization for Standardization, Geneva, Switzerland.
15. Alves, L.M., Afonso, R.M., Martins, P.A.F., 2020, Double-sided self-pierce riveting. *International Journal of Advanced Manufacturing Technology*, 108, 1541-1549.
16. Alves, L.M., Afonso, R.M., Pereira, P.T., Martins, P.A.F., 2021, Double-sided self-pierce riveting of dissimilar materials. *International Journal of Advanced Manufacturing Technology*, 115, 3679–3687.
17. ISO 14273:2000(E), 2000, *Specimen dimensions and procedure for shear testing resistance spot, seam and embossed projection welds.* ISO - International Organization for Standardization, Geneva, Switzerland.
18. Nielsen, C.V., Martins, P.A.F., 2021, Finite element simulation: A user's perspective In: *Metal forming: formability, simulation and tool design*. Academic Press, London. (https://doi.org/10.1016/B978-0-323-85255-5.00011-X)
19. Mattiasson, K., 2010, FE-models of the sheet metal forming processes. In: Banabic, D. (Ed.), *Sheet Metal Forming Processes: Constitutive Modelling and Numerical Simulation*. Springer, Berlin.
20. Nielsen, C.V., Zhang, W., Alves, L.M., Bay, N., Martins, P.A.F., 2013, Coupled finite element flow formulation In: (Ed. Davim, J.P.) *Modelling of thermo-electro-mechanical manufacturing processes with applications in metal forming and resistance welding*. Springer, New York. (https://doi.org/10.1007/978-1-4471-4643-8_3).